Directed Assembly of Metal Nanoparticles in Polymer Bilayers

Su-Wen Hsu[1], Yuhan Long[2], Aatheya G. Subramanian[2], and Andrea R. Tao[1,2]

[1]NanoEngineering Department, University of California, San Diego

9500 Gilman Drive MC 0448, La Jolla, CA 92093-0448

[2]Materials Science and Engineering, University of California, San Diego

9500 Gilman Drive MC 0448, La Jolla, CA 92093-0448

*E-mail: atao@eng.ucsd.edu

Abstract:

The integration of layer-by-layer (LbL) and self-assembly methods has the potential to achieve precision assembly of nanocomposite materials. Knowledge of how nanoparticles move across and within stacked materials is critical for directing nanoparticle assembly. Here, we investigate nanoparticle self-assembly within two different LbL architectures: (1) a bilayer composed of two immiscible polymer thin-films, and (2) a bilayer composed of polymer and graphene that possesses a “hard-soft” interface. Polymer-grafted silver nanocubes (AgNCs) are employed as a model nanoparticle system for systematic experiments – characterizing both assembly rate and

resulting morphologies – that examine how assembly is affected by the presence of an interface. We observe that polymer grafts can serve to anchor AgNCs at the bilayer interface and to decrease particle mobility, or can promote particle transfer between layers. We also find that polymer viscosity and polymer mixing parameters can be used as predictors of assembly rate and behavior. These results provide a pathway for designing more complex multilayered nanocomposites.

Introduction

Layer-by-layer (LbL) methods offer a facile, modular approach for creating stacked thin-film architectures.[1] For example, spin-coating, electrospray deposition, and immersive coating have been used to deposit multilayers composed of a wide range of materials including polymers,[2-4] colloidal particles,[5-7] and biomolecules.[8] LbL deposition is a general and versatile approach for constructing complex, functional materials where multilayer coatings are built up to form bilayers or stacks that can be several millimeters thick. LbL methods have been well-developed for the controlled deposition of polymer and polyelectrolyte multilayers, with layers as thin as 2 nm and low surface roughness.[1]

While LbL methods have also been widely demonstrated for the fabrication of nanoparticle (NP) layers from colloidal dispersions, the degree of control over layer morphologies is varied. For example, spin-casting yields precise control over NP layer thicknesses,[5] but typically results in dense and disordered NP assembly within each layer. NP thin-film coatings have also been demonstrated using immersion coating, where a host substrate is immersed in alternating solutions of oppositely-charged NPs or polyelectrolytes.[6, 9, 10] While the stability of the multilayer structure is extremely high due the strong electrostatic adhesion between oppositely charged NPs, immersion deposition often leads to porous or low-density NP layers. The presence of a large number of interstitial voids within the layer can lead to poor layer stratification and the formation of interpenetrating NP layers. Few LbL methods can achieve the high degree of control over NP placement, arrangement, and orientation required for advanced nanomanufacturing.

Self-assembly provides a powerful approach for organizing nanocomponents on a massively parallel scale and with the potential for nanoscale precision. Several strategies have been developed for achieving controlled assembly of nanoparticle (NP) building blocks, including the use of DNA linkers, grafted polymers, fluidic assembly, patterned surfaces, and external forces.[11-16] NPs incorporated into polymers are especially attractive as they allow for facile device integration using techniques that take advantage of batch, low-cost processing and enable the fabrication of state-of-the-art nanocomposites. Typically, nanocomposites are formed by introducing filler NPs, usually surface-modified with polymers grafts to prevent nonspecific aggregation into a host polymer at specific loading densities. NP assembly proceeds by phase segregation into NP-rich domains upon temperature and/or solvent annealing.[17-20] This dynamic segregation can be frozen at a specific stage of assembly to trap a desired NP structure and to prevent further domain coarsening.[21, 22] Thus, the ability to encapsulate NPs into polymers has the potential to harness the rich phase behavior exhibited by this multi-component system of NPs, NP grafts, and matrix polymer.

A fabrication approach that harnesses the capabilities of both layer-by-layer deposition and polymer-directed self-assembly has the potential to achieve precise control over nanocomposite organization. To provide a first demonstration of this, we investigate the self-assembly mechanism and architectures for polymer-grafted metal NPs deposited in a LbL fashion at two different kinds of bilayers: (i) a polymer-polymer interface and (ii) a polymer-graphene interface. Figure 1 shows a schematic of these two different systems. The first is comprised of two immiscible polymer thin-films, polystyrene (PS) and poly (methyl methacrylate) (PMMA), fabricated by spin-coating. The second

system consists of a unique “hard-soft” interface where monolayer graphene is deposited by a wet transfer method onto a PS thin-film.[23] The interactions (both intermolecular[24, 25] and interparticle) within the resulting bilayer nanocomposites can be tuned to adjust the location of NP within the bilayer, interparticle orientation, and rate of NP assembly.

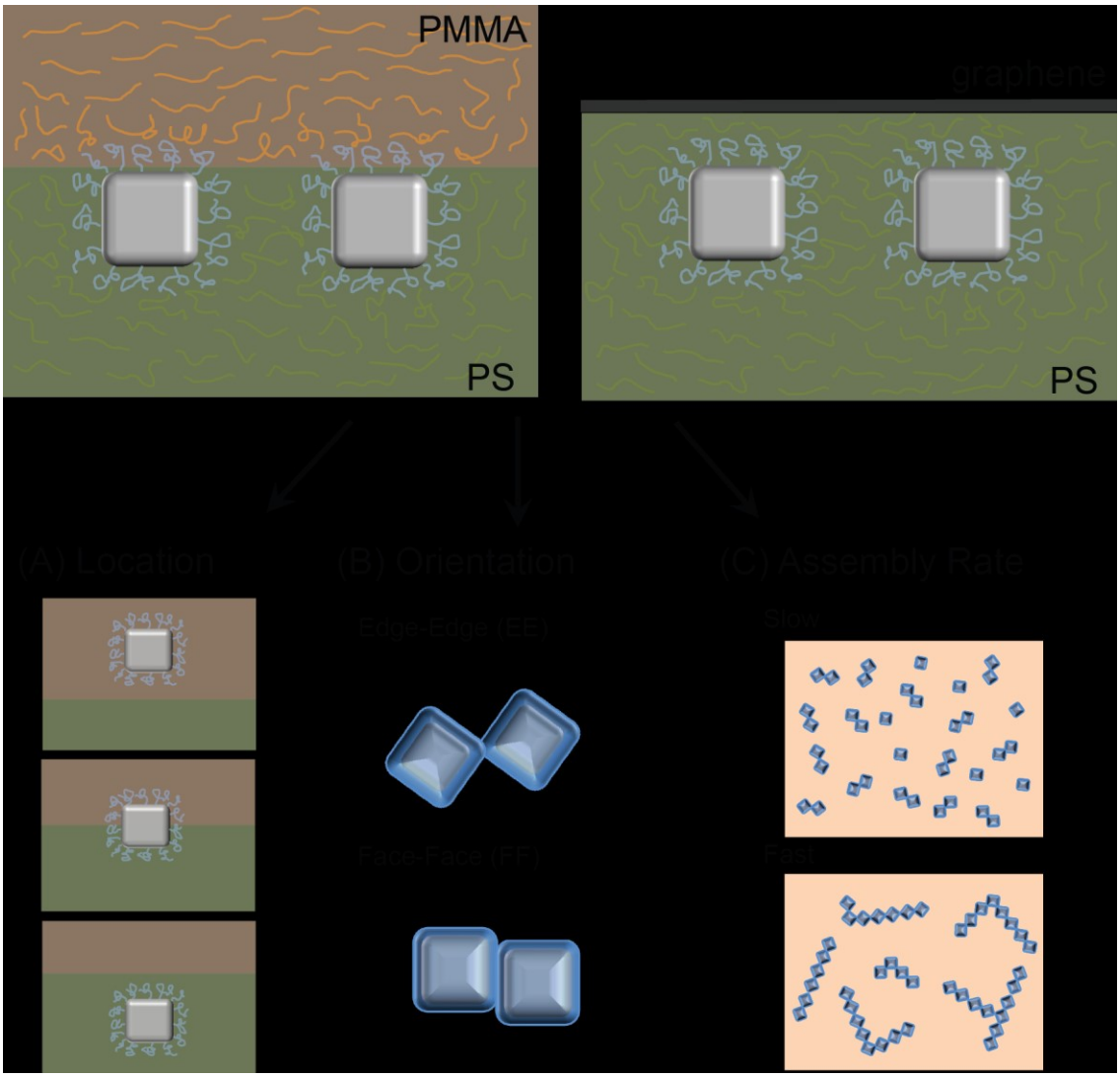

Figure 1. Schematic of shaped NPs embedded into two bilayer systems, PS-PMMA and PS-graphene. The multiple interactions between NPs, polymer grafts, and matrix polymers can be used to tune: (a) NP location within the bilayer stack, (b) interparticle orientation, (c) and rate of self-assembly to form NP clusters or larger NP-rich domains.

Results & Discussion

Figure 2 shows a schematic of the four LbL steps for fabricating the bilayer nanocomposites. First, a 200 nm thin-film of PS (M_n= 11500) is spin-coated onto a solid Si support from a toluene solution. Second, polymer-grafted Ag nanocubes (AgNCs) are transferred onto the PS thin-film by Langmuir-Blodgett (LB) deposition. AgNC were chosen as the NP component because they have been demonstrated to undergo polymer-directed phase segregation and because they possess a well-defined shape that enables analysis of NP assembly by quantitative image analysis.[26-28] The AgNCs are approximately 75 nm in edge length and form a well-dispersed, near hexagonal arrangement when transferred onto the PS surface. The third step is a thermal treatment that embeds the AgNCs into the underlying PS layer. This is achieved by heating the film to 110°C, well above the T_g of PS. Our experiments indicate that after thermal treatment for 30 min, the AgNCs are fully embedded into the PS layer but remain relatively close (within 10 nm) to the PS-air interface. (See supporting information) In the fourth step, the second layer -- either PMMA or graphene -- is deposited onto the PS surface. For PMMA, a 150-200 nm thin-film is deposited by spin-coating from acetonitrile solution. For graphene, transfer is achieved by starting with a monolayer of graphene grown by chemical vapor deposition on top of a Cu support (Grolltex, Inc) and coated with a sacrificial PMMA layer. The monolayer graphene transfer includes (1) etching the Cu support in a 0.25 M $FeCl_3$ solution, (2) rinsing in DI water, (3) transferring onto the PS substrate, and then (4) dissolving the PMMA film by acetone. Finally, the AgNCs are assembled by heating the entire bilayer nanocomposite above the T_g of PS for an

extended period of time to allow AgNC diffusion and, ultimately, phase segregation of AgNC-rich domains.

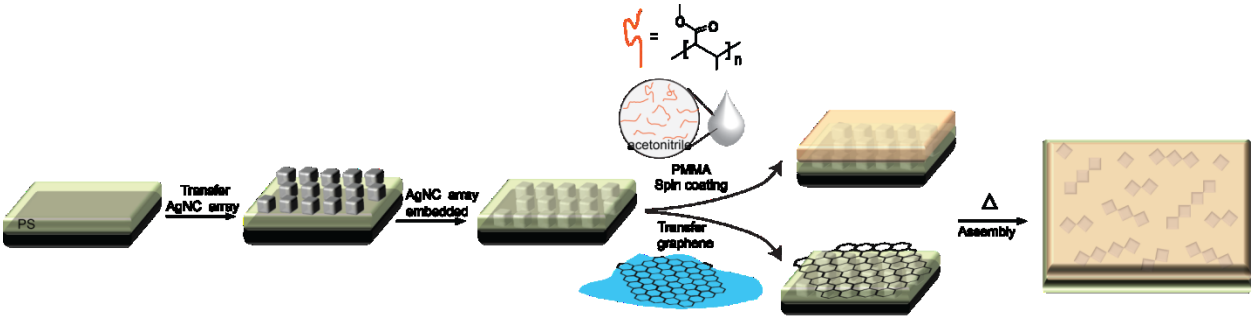

Figure 2 Schematic of the LbL fabrication process for the bilayer nanocomposites, including: transfer of AgNCs to the PS substrate, embedding the AgNCs into the PS layer, deposition of either PMMA or graphene, and thermal treatment to instigate phase segregation.

First, we investigated the effect of the bilayer interface on AgNC assembly in comparison to the air-PS interface. AgNCs grafted with polyvinyl pyrrolidone (PVP) were embedded into three different architectures: a single layer of PS (M_w=11500K), a PS-PMMA (M_w=17000) bilayer, and a PS-graphene bilayer. AgNC assembly was carried out at T= 130°C, which is above the T_g of both the PS (T_g=105°C) and PMMA (T_g= 110°C). Upon thermal treatment, the AgNCs assemble into chain-like structures with varying lengths. Assembly was monitored observing samples by scanning electron microscopy (SEM) with increasing thermal treatment times (See supporting information, S2). Figure 3 shows SEM images of the embedded and assembled AgNCs in PS, PS-PMMA, and PS-graphene after 8h of thermal treatment. Assembly rate was measured by analyzing these SEM images with the “Particle Image Characterization Tool (PICT)” developed in our previous work[28] to calculate the average number (N) of AgNCs per chain. Figure 3

shows *N* plotted with respect to time. The nonlinear growth rate observed for all three architectures is consistent with step-wise growth described in previous reports.[29] Assembly within the single PS layer occurs the fastest, followed by the PS-graphene bilayer; the PS-PMMA bilayer exhibits the slowest rate of AgNC assembly. Each dataset shows a best fit to the exponential expression, $N = N_o + Ae^{rt}$ where N_o is related to initial dispersity of the AgNCs (N =1 at t=0 for a perfect dispersion), *A* is a pre-exponential factor related to NP mobility, and the r is a growth constant. The fit parameters for each of the curves shown in Figure 3 are given in Table 1. All three architectures exhibit similar *r* values, suggesting that the overall growth constant is not affected by the bilayer architecture. This suggests that assembly rate is primarily dictated by lateral mobility of the AgNCs within the polymer layers.

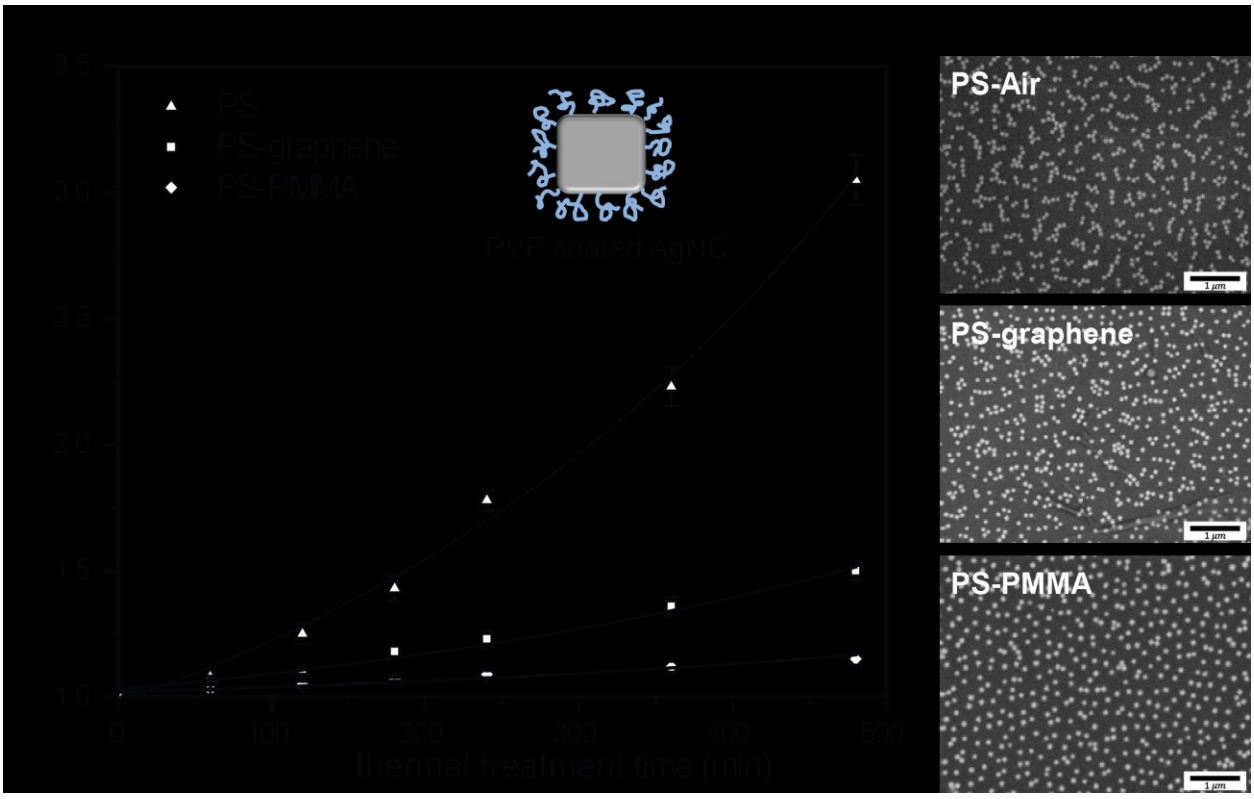

Figure 3. Assembly rate is measured by plotting the average N with thermal treatment time for PS and bilayer systems. Solid lines show fitted curves for each dataset. SEM images show the nanocubes assembled in PS, PS-graphene, and PS-PMMA system after 8h thermal treatment.

Table 1 : Exponential fit for datasets in Figure 3, measuring N with respect to time, t.

Shell of AgNC	PS			PS-PMMA			PS-graphene		
	N_0	A	r	N_0	A	r	N_0	A	r
PVP	0.181	0.800	0.0027	0.938	0.082	0.0024	0.782	0.247	0.0023
PEG-SH	0.930	0.132	0.0022	0.975	0.044	0.0029	0.972	0.048	0.0024
Dodecanethiol	0.083	0.913	0.0097	1.043	0.243	0.0079	0.797	0.265	0.0072

Rate of AgNCs assembled presents as $N = N_o + Ae^{rt}$

A: Related to lateral diffusion rate of AgNCs or AgNC collision frequency.

r: Growth constant for AgNC domains.

For the PS-PMMA bilayer, cross-sectional SEM images show that AgNCs remain close to the bilayer interface but remain almost fully embedded in the PS layer during the assembly process. This suggests that reduced AgNC mobility within the PS-PMMA bilayer may result from two effects: (i) an increase in the T_g of the interfacial PS layer where the AgNCs reside, or (ii) strong AgNC ligand interactions with the PMMA layer that effectively pin the AgNCs and discourage lateral diffusion. This first effect would decrease AgNC mobility by slowing the lateral diffusion of the PS matrix polymer. While this has been observed for immiscible polymer bilayers,[30] it is unlikely that this interfacial effect would extend >70 nm into the PS film to significantly affect lateral AgNC diffusion.

To further investigate these effects, we observed AgNC assembly for PS-PMMA bilayers where we systematically vary the viscosity, η of the PMMA layer in the range of 10^2-10^4 Pa·S (See supporting information, S3). Figure 4 plots *N* versus assembly time for these different bilayers and shows the corresponding SEM images after 8h of thermal treatment. Compared to assembly rate in single-layer PS (dashed line), the rate of AgNC assembly decreases dramatically with increased η. Exponential fitting shows that this is primarily due to a change in the pre-exponential A-value, which is reduced by as much as 50 times for η=25800 Pa·s. This significant decrease suggests that the PVP ligands grafted at the AgNC surface extend across the bilayer interface into the PMMA layer, effectively anchoring the AgNCs and slowing the assembly process.

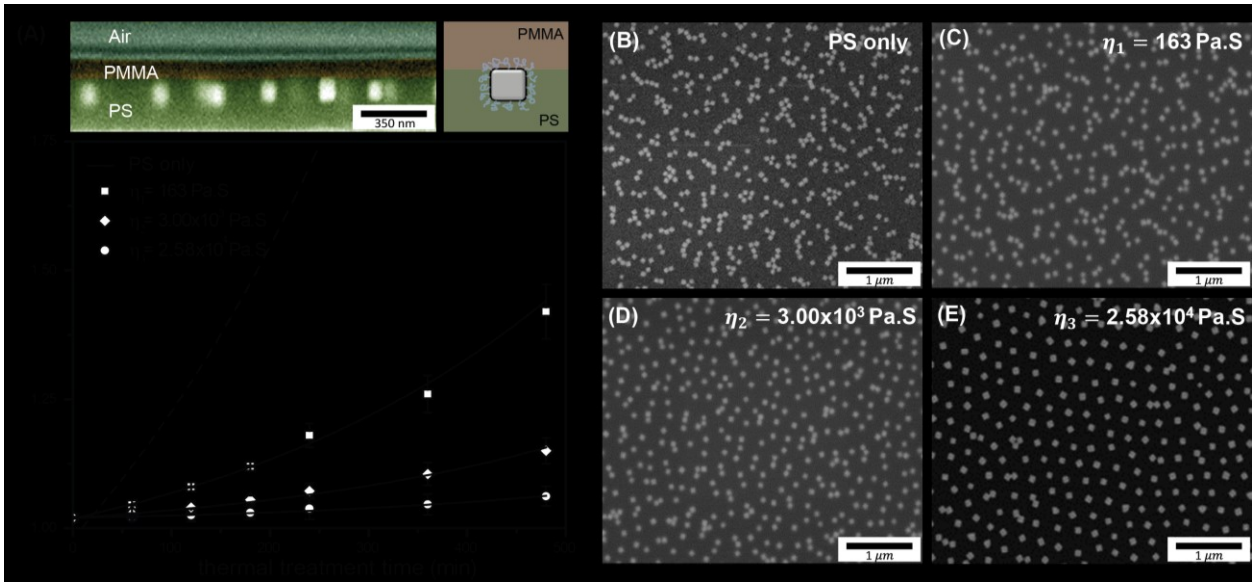

Figure 4. Rate of assembly for PVP-grafted AgNCs assembled in PS-PMMA bilayers with respect to PMMA viscosity. (A) The cross-sectional SEM shows the nanocube located near the PS (green color)-PMMA (orange color) interface but still embedded within the PS layer. Assembly ate was quantified by measuring N as a function of time for three different viscosities of PMMA: η_1=163 Pa·S (square), η_2= 3x10^3 Pa·S (rhombus), and η_3= 2.58x10^4 Pa·S (circle). Shown for comparison

is the growth curve for single-layer PS, with no PMMA layer (dashed line). The SEM images show the AgNCs assembled after 8h of thermal treatment in (B-E), respectively.

For AgNCs assembled in PS-graphene, cross-sectional images show that the AgNCs remain close to the bilayer interface, but undergo rotation away from the interface during the assembly process. (Fig. 5A) SEM images (Fig 5B-E) before and after thermal treatment indicate that as assembly progresses, the population of rotated AgNC (e.g. with facets that are not parallel to the bilayer) increases (red circles). This provides a qualitative explanation of the assembly rate observed for the PS-graphene bilayer: the unfavorable interaction between PVP ligands and graphene cause the AgNCs move away from the interface through this rotation. This frees the AgNCs to diffuse and assemble since the PVP ligands are no longer anchored at the interface.

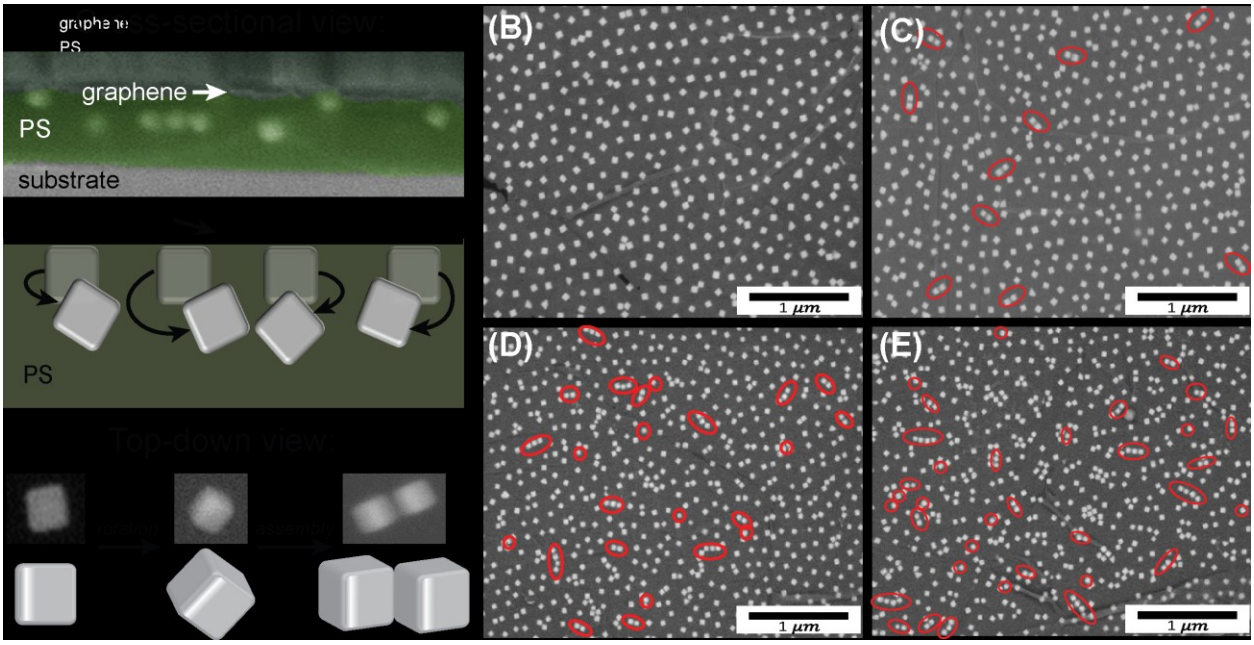

Figure 5 AgNCs assembled in the PS-graphene bilayer. (A) Side-view: the cross-sectional SEM shows the AgNCs are located buried in the PS layer, leading to NP rotation as top-view SEM images show the square facet of AgNC is not parallel to the bilayer interface. The SEM images

show the assembled AgNCs for thermal treatment times of t= 0, 3h, 6h, 8h in panels (B-E), respectively. Red circles indicate AgNCs that have undergone rotation away from the bilayer interface.

In further support of chemical anchoring across the bilayer interface, we carried out assembly experiments for AgNCs grafted with 1-dodecanethiol and thiol-termianted poly(ethylene glycol) (PEG) (M_w=20000). Figure 6 plots *N* with respect to thermal treatment time. We expected assembly rate to be the highest for AgNC grafts that are miscible with PS and do not interact with the second layer, whereas the slowest assembly rate is expected for AgNC grafts that are miscible with the second layer that results in an anchoring effect. To approximate the miscibility of the AgNC ligands within the bilayer, we can refer to the Flory-Huggins interaction parameter, χ. On the PS side of the bilayer, we expect the miscibility of PEG grafts to be poorer than that of PVP, since $\chi_{PS\text{-}PVP}$=0.033 and $\chi_{PS\text{-}PEG}$=0.064.[31, 32] For 1-dodecanethiol, we can estimate (based on knowledge of alkane mixing) the value of χ to be ~0.016.[33] On the PMMA side of the bilayer, $\chi_{PMMA\text{-}PEG}$= -0.005,[34] indicating miscibility, whereas $\chi_{PVP\text{-}PMMA}$= 0.007 and $\chi_{PMMA\text{-}alkane}$=1.24,[32, 35] indicating high immiscibility between PMMA and the alkane grafts.

We observe similar kinetics in both bilayer cases: assembly rate for AgNCs modified with PEG grafts is slower than for PVP grafts, and assembly rate is fastest for the alkane grafts. Interestingly, we observe that the PEG-grafted AgNCs move across the bilayer into the top PMMA layer. For the PS-graphene bilayer, there is little driving force for the AgNCs to move across or even near the bilayer interface, as evidenced by the cross-sectional SEM image in Figure 6. On the other hand, alkane-grafted AgNCs stay buried in the PS layer and undergo fast assembly. SEM images confirm that the alkane

grafts enable maximum interparticle attraction, evidenced by the dominance of face-face interparticle orientations. This is consistent with previous studies showing that shorter grafts lengths promote face-face assembly configurations.[26]

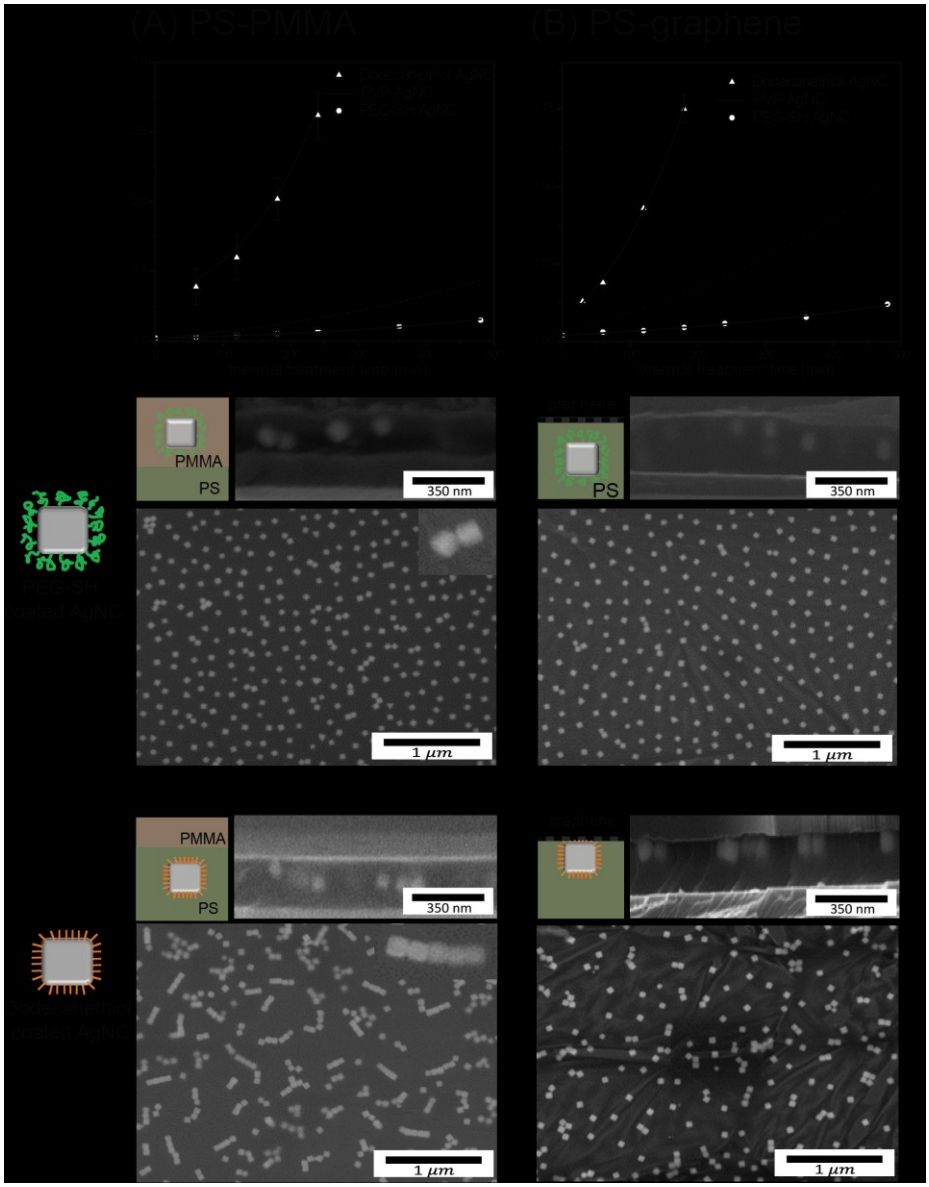

Figure 6 Growth curves for AgNCs assembled in (A) PS, (B) PS-PMMA, and (C) PS-graphene layers and grafted with PVP (dashed), PEG (circles), and 1-dodecanethiol (triangles). The cross-

sectional and top-down SEM images show the location and orientation of the AgNCs in each combination of surface chemistries and bilayer architectures.

Conclusions

Within LbL deposited bilayers, our results indicate that NP assembly can be greatly affected by neighboring polymer domains due to strong graft-polymer interactions, even when a distinct bilayer interface exists. Selection of polymer grafts based on mixing behavior can be used to program the location of NPs and assembly rate within the bilayer. The ability to selectively anchor (with polymer grafts) and pin (with graphene) NPs in the polymer layer of choice also has promise in the generation of multi-stacked architectures, where sequential layer deposition and polymer processing may cause disorder by allowing NP diffusion within and across layers. The use of graphene as a boundary layer also holds promise in designing LbL stacks without the need for developing orthogonal polymer chemistries and processing steps. Our results provide a pathway to designing more complex nanostructured multilayers and NP-polymer blends, opening new avenues in the structural design of multicomponent and multifunctional nanocomposites that have potential applications in advanced surface coatings for broadband optical absorption or reflection, enhanced polymer adhesion, and device packaging.

Acknowledgements

This work was supported through a grant from National Science Foundation (CMMI Award 1636356). We acknowledge UCSD’s Nano3 facility for use of their scanning electron microscope facility. We also thank Dr. Gaurav Arya for helpful discussion.

References

1. Richardson, J. J.; Björnmalm, M.; Caruso, F. *Science* **2015,** 348, (6233), aaa2491.
2. Schlenoff, J. B.; Dubas, S. T.; Farhat, T. *Langmuir* **2000,** 16, (26), 9968-9969.
3. Hoogeveen, N. G.; Cohen Stuart, M. A.; Fleer, G. J.; Böhmer, M. R. *Langmuir* **1996,** 12, (15), 3675-3681.
4. Kim, J. Y.; Kim, B. H.; Hwang, J. O.; Jeong, S. J.; Shin, D. O.; Mun, J. H.; Choi, Y. J.; Jin, H. M.; Kim, S. O. *Advanced Materials* **2013,** 25, (9), 1331-1335.
5. Thomas, I. M. *Appl. Opt.* **1987,** 26, (21), 4688-4691.
6. Lee, D.; Rubner, M. F.; Cohen, R. E. *Nano Letters* **2006,** 6, (10), 2305-2312.
7. Malikova, N.; Pastoriza-Santos, I.; Schierhorn, M.; Kotov, N. A.; Liz-Marzán, L. M. *Langmuir* **2002,** 18, (9), 3694-3697.
8. Picart, C.; Lavalle, P.; Hubert, P.; Cuisinier, F. J. G.; Decher, G.; Schaaf, P.; Voegel, J. C. *Langmuir* **2001,** 17, (23), 7414-7424.
9. Srivastava, S.; Kotov, N. A. *Accounts of Chemical Research* **2008,** 41, (12), 1831-1841.
10. Jiang, C.; Markutsya, S.; Tsukruk, V. V. *Advanced Materials* **2004,** 16, (2), 157-161.
11. Nykypanchuk, D.; Maye, M. M.; van der Lelie, D.; Gang, O. *Nature* **2008,** 451, (7178), 549-552.
12. Park, S. Y.; Lytton-Jean, A. K. R.; Lee, B.; Weigand, S.; Schatz, G. C.; Mirkin, C. A. *Nature* **2008,** 451, (7178), 553-556.
13. Lin, Y.; Boker, A.; He, J.; Sill, K.; Xiang, H.; Abetz, C.; Li, X.; Wang, J.; Emrick, T.; Long, S.; Wang, Q.; Balazs, A.; Russell, T. P. *Nature* **2005,** 434, (7029), 55-59.
14. Akcora, P.; Liu, H.; Kumar, S. K.; Moll, J.; Li, Y.; Benicewicz, B. C.; Schadler, L. S.; Acehan, D.; Panagiotopoulos, A. Z.; Pryamitsyn, V.; Ganesan, V.; Ilavsky, J.; Thiyagarajan, P.; Colby, R. H.; Douglas, J. F. *Nat Mater* **2009,** 8, (4), 354-359.
15. Shenhar, R.; Norsten, T. B.; Rotello, V. M. *Advanced Materials* **2005,** 17, (6), 657-669.

16. Kim, J. Y.; Kim, H.; Kim, B. H.; Chang, T.; Lim, J.; Jin, H. M.; Mun, J. H.; Choi, Y. J.; Chung, K.; Shin, J.; Fan, S.; Kim, S. O. *Nature Communications* **2016,** 7.
17. Ajayan, P. M.; Schadler, L. S.; Braun, P. V., *Nanocomposite science and technology*. John Wiley & Sons: 2006.
18. RamanathanT; Abdala, A. A.; StankovichS; Dikin, D. A.; Herrera Alonso, M.; Piner, R. D.; Adamson, D. H.; Schniepp, H. C.; ChenX; Ruoff, R. S.; Nguyen, S. T.; Aksay, I. A.; Prud'Homme, R. K.; Brinson, L. C. *Nat Nano* **2008,** 3, (6), 327-331.
19. Saunders, B. R.; Turner, M. L. *Advances in Colloid and Interface Science* **2008,** 138, (1), 1-23.
20. Mackay, M. E.; Tuteja, A.; Duxbury, P. M.; Hawker, C. J.; Van Horn, B.; Guan, Z.; Chen, G.; Krishnan, R. S. *Science* **2006,** 311, (5768), 1740-1743.
21. Galush, W. J.; Shelby, S. A.; Mulvihill, M. J.; Tao, A. R.; Yang, P.; Groves, J. T., Plasmonic System for Detecting Binding of Biological Molecules. US Patent App. 13/204,506: 2011.
22. Wong, H. C.; Cabral, J. T. *Phys. Rev. Lett.* **2010,** 105, 038301-038304.
23. Suk, J. W.; Kitt, A.; Magnuson, C. W.; Hao, Y. F.; Ahmed, S.; An, J. H.; Swan, A. K.; Goldberg, B. B.; Ruoff, R. S. *Acs Nano* **2011,** 5, (9), 6916-6924.
24. Jin, H. M.; Park, D. Y.; Jeong, S. J.; Lee, G. Y.; Kim, J. Y.; Mun, J. H.; Cha, S. K.; Lim, J.; Kim, J. S.; Kim, K. H.; Lee, K. J.; Kim, S. O. *Advanced Materials* **2017,** 29, (32).
25. Kim, J. Y.; Lim, J.; Jin, H. M.; Kim, B. H.; Jeong, S. J.; Choi, D. S.; Li, D. J.; Kim, S. O. *Advanced Materials* **2016,** 28, (8), 1591-1596.
26. Gao, B.; Arya, G.; Tao, A. R. *Nature Nanotechnology* **2012,** 7, (7), 433-437.
27. Gurunatha, K. L.; Marvi, S.; Arya, G.; Tao, A. R. *Nano Letters* **2015,** 15, (11), 7377-7382.
28. Murthy, C. R.; Gao, B.; Tao, A. R.; Arya, G. *Physical Review E* **2016,** 93, (2).
29. Bigioni, T. P.; Lin, X. M.; Nguyen, T. T.; Corwin, E. I.; Witten, T. A.; Jaeger, H. M. *Nature Materials* **2006,** 5, (4), 265-270.

30. Roth, C. B.; McNerny, K. L.; Jager, W. F.; Torkelson, J. M. *Macromolecules* **2007,** 40, (7), 2568-2574.
31. Dai, K. H.; Kramer, E. J. *Polymer* **1994,** 35, (1), 157-161.
32. Walheim, S.; Ramstein, M.; Steiner, U. *Langmuir* **1999,** 15, (14), 4828-4836.
33. Hermes, H. E.; Higgins, J. S.; Bucknall, D. G. *Polymer* **1997,** 38, (4), 985-989.
34. Cimmino, S.; Martuscelli, E.; Silvestre, C. *Polymer* **1989,** 30, (3), 393-398.
35. Zsoldos, G. E.; Kollar, M. *Journal of Thermal Analysis and Calorimetry* **2015,** 119, (1), 63-72.